Article:
Cao, T., Lü, B., Xu, D. et al. (4 more authors) (2015) An efficient method for thickness prediction in multi-pass incremental sheet forming. International Journal of Advanced Manufacturing Technology, 77 (1-4). 469 - 483. ISSN 0268-3768

https://doi.org/10.1007/s00170-014-6489-9

Int J Adv Manuf Technol (2015) 77:469–483
DOI 10.1007/s00170-014-6489-9

Received: 3 June 2014 /Accepted: 9 October 2014
Published online: 18 October 2014

An efficient method for thickness prediction in multi-pass incremental sheet forming

Tingting Cao[a], Bin Lu[a,b*], Dongkai Xu[a], Huan Zhang[a], Jun Chen[a], Hui Long[b], Jian Cao[c]

[a] Department of Plasticity Technology, Shanghai Jiao Tong University, 1954 Huashan Road, Shanghai, 200030, P.R. China
[b] Department of Mechanical Engineering, The University of Sheffield, , Sheffield, S1 3JD, UK
[c] Department of Mechanical Engineering, Northwestern University, Evanston, IL 60208, USA

* Corresponding author: bin_lu@sjtu.edu.cn

Abstract

Incremental sheet forming (ISF) is a highly versatile and flexible process for rapid manufacturing of complex sheet metal parts. In the ISF process, efficient and accurate prediction of part thickness variation is still a challenging task, which is especially true for the multi-pass ISF process. The Sine law equation and the finite element method (FEM) are the two commonly used conventional prediction methods. However, these approaches are either with limited accuracy or very time consuming. For the multi-pass ISF process, the thickness prediction is even more challenging since two or more forming steps are involved. Focusing on the thickness prediction of multi-stage ISF process, this work proposes a thickness prediction model based on the geometrical calculation of intermediate shapes of the formed part and backward tracing of nodal points of the forming tool. By developing this method, the thickness distribution can be calculated through the predicted nodal displacement in the ISF process. To verify the proposed model, four different geometrical shapes, i.e. conic, parabolic conic, non-axisymmetric and hemispherical parts, are physically formed by using a NC ISF machine. The geometric shapes and the detailed thickness distributions of the formed parts are carefully measured and compared with the prediction model developed. Good agreements between the analytical predictions and the experimental results are obtained. This indicates the effectiveness and robustness of the developed thickness prediction approach.

Keywords

Incremental Sheet Forming, Multi-pass Forming, Thickness Prediction

Int J Adv Manuf Technol (2015) 77:469–483
DOI 10.1007/s00170-014-6489-9

Received: 3 June 2014 /Accepted: 9 October 2014
Published online: 18 October 2014

1. Introduction

Incremental sheet forming (ISF) is an advanced flexible sheet forming process. By using this process, a 3D complex freeform part can be produced by driving a simple stylus-type tool over a predefined tool path. As dedicated forming tool sets with specific shapes are not necessary in this process, it can effectively shorten the lead time and reduce the production cost[1]. Meanwhile, ISF technology also exhibits higher formability comparing to the conventional sheet forming processes. This may be due to its localized and incremental deformation nature, which avoids sheet necking that normally occurs in conventional sheet forming processes such as deep drawing [2]. Furthermore, the ISF forming force is usually low due to its localized deformation nature. This reduces the size and capacity of forming machines needed. Considering these advantages, ISF becomes a good alternative to the conventional sheet forming processes in manufacturing small batch or customized sheet components, such as in the product development process of aerospace [1], biomedical [3] and automotive sectors [4].

The original ISF technology, a single point incremental forming (SPIF) process was first proposed by Iseki et al. [5] in association of cutting expensive stamping dies in the manufacturing of a car body panel. Based on the SPIF technology, variants of the ISF processes have been developed, such as the two-point incremental forming (TPIF) [6], double side incremental forming (DSIF) [7], laser assisted incremental forming [8], electric hot incremental forming [9] and water jet incremental sheet bulging method [10]. Due to these developed ISF processes, components with complex shapes and hard-to-form materials can be produced successfully, which further expands the application fields of the ISF technology.

Although the ISF technology shows better formability, components with steep wall angles or vertical wall are still difficult to be formed in a single pass. This is due to the localized deformation nature of ISF: the material deformation occurs only in a small area that contacts with the forming tool and the surrounding material cannot be drawn into the deformation zone to compensate for the local material insufficiency. To overcome this problem, multi-pass ISF process has been developed to redistribute the material uniformly by proposing different forming strategies [11]. In the multi-pass ISF, if the forming strategy is

Int J Adv Manuf Technol (2015) 77:469–483
DOI 10.1007/s00170-014-6489-9

Received: 3 June 2014 /Accepted: 9 October 2014
Published online: 18 October 2014

well designed, more uniform thickness distribution can be obtained and parts with steeper wall angles may be produced without crack failure. Skjoedt et al. [12] obtained a circular cylindrical cup with vertical wall angle by two different five-pass forming strategies. Malhotra et al.[13] proposed a mixed tool path strategy to achieve a smoother component base by using a combination of in-to-out and out-to-in tool paths for each intermediate shape. Using this strategy, a cylindrical cup with the stepped features could be generated. These examples demonstrate the advances of multi-pass ISF process.

In the multi-pass ISF process, the forming strategy, especially intermediate shapes, will significantly affect the maximum achievable forming angle. However, the design of intermediate shapes is mainly based on the designer's experience [14]. Thickness prediction in multi-pass ISF plays a significant role in design optimization of intermediate shapes. In this way, how to predict the thickness distribution becomes a major challenge in multi-pass ISF process design. However, although many efforts have been made to improve the thickness uniformity using multi-pass ISF, there is no systematic approach for the prediction of thickness distribution. Fast prediction of thickness distribution of ISF parts is still a challenging task in multi-pass ISF process.

In the conventional single-pass ISF process, thickness prediction can be obtained through the Sine law model [15]. However, this approach has very limited accuracy. Furthermore, the Sine law may not be used for the thickness prediction in multi-pass ISF process. This was proven in the Kitazawa and Nakanes' work [16], in which the thickness distribution of the hemispheric shaped component formed by two-pass incremental forming was significantly different from the result of using Sine law. Kitazawa et al. [17] also demonstrated that the thinning of sheets in multi-pass incremental forming could exceed the maximum thickness reductions observed in single-pass processing.

Another possible approach for thickness prediction is the finite element method (FEM). By employing both FEM and physical experiments, He et al. [18] compared the numerical and experimental results for forming of an aluminum cone with 50° wall angle. Good agreement with a maximum difference of less than 0.1mm was obtained in their work. However, the FE approach is very time consuming, especially for multi-pass ISF process. In order to effectively predict the thickness distribution, Bambach [19] proposed a geometrical approach, in which

Int J Adv Manuf Technol (2015) 77:469–483
DOI 10.1007/s00170-014-6489-9

Received: 3 June 2014 /Accepted: 9 October 2014
Published online: 18 October 2014

the material points were assumed to be moved along the normal direction of the transient surface point of geometrical shape. The above approaches concentrate on ISF within a single pass, but the thickness prediction methods for multi-pass forming are rarely explored.

Concerning the current research related to multi-pass ISF process, Duflou et al. [20] investigated the difference of material deformation between multi-pass and single pass ISF. Filice [21] proposed an analytical model to predict the thickness distribution using the geometry shape parameter of the final formed parts in a double-pass incremental forming of a cylindrical cup. Other than the above works, there are only limited researches investigate thickness prediction. The lack of understanding in the material deformation and thickness distribution becomes a barrier in multi-pass ISF design, especially for the determination of intermediate shapes and pass numbers.

Focusing on the prediction of thickness distribution in the multi-pass ISF process, a geometrical approach has been proposed in this work. In the calculation, the nodal positions on the geometric profiles are tracked for each z-level generated based on the geometry of the tool path, the tool radius and the tool step down value. Based on the calculated nodal displacement, the thickness distribution can be calculated according to the principle of volume constancy. Using the developed method, four examples of forming parts with different geometrical shapes are studied, in which the geometric profiles and thickness distributions of the formed shapes are measured to be compared with the predicted results. This is followed by the discussion and conclusion of the developed approach.

2. Methodology

Concerning the material deformation in the SPIF process, although the tool moves along the circumferential direction, there is only limited circumferential strain while the dominant material deformation occurs in the meridional direction. In most cases, the SPIF process can be considered under plane-strain condition in the plane perpendicular to the tool movement direction. The plane-strain deformation was observed in many researches. He et al. [22] found that the tangential strain in incremental forming of a cone was much smaller as compared to the strain in the radial direction. Ji and Park [23] also found that the circumferential strain was

Int J Adv Manuf Technol (2015) 77:469–483
DOI 10.1007/s00170-014-6489-9

Received: 3 June 2014 /Accepted: 9 October 2014
Published online: 18 October 2014

small enough to be negligible in SPIF process. Fang et al. [24] measured the sheet deformation during the SPIF experiment and found that the meridional strain was 15-20 times larger than the circumferential strain. However, in the case when the circumferential curvature increases, the material deformation does not follow the plane strain assumption any more [19]. For parts such as pyramid with small corners, the sheet deformation is under biaxial stretching deformation condition. By considering the general ISF deformation conditions and ignoring the through thickness shear effect and the case of corner deformation, the plain-strain assumption is made in the analysis. In this way, the tracing of material points on the surface of a part can be implemented in the 2D cross-sections of the part. In addition, other assumptions include: a) the material volume is constant; b) the bending effect is ignored. Based on these assumptions, a thickness prediction model for the multi-pass incremental forming is proposed. This thickness prediction model includes three key steps: (1) Prediction of geometric profiles for each pass; (2) Tracing the material points on the part surface; (3) Calculating the thickness distribution. The detail calculation of thickness distribution is given as follows.

2.1 Description of the 2D cross-section profiles

In this work, the geometric cross-section profiles of forming parts are described by using rational Bezier curves. Rational Bezier curve is a parametric polynomial curve, which does not involve complex geometrical calculation and is especially suitable for describe the cross-section of ISF parts. In the calculation, a rational Bezier curve in n^{th} degree can be defined by [25]:

$$C(u)=\frac{\sum_{i=0}^{n} B_{i,n}(u)\omega_i P_i}{\sum_{i=0}^{n} B_{i,n}(u)\omega_i} \qquad 0\le u\le 1 \tag{1}$$

where $P_i=(x_i,y_i,z_i)$ is control point and ω_i is the scalar for each point. In the equation, the basis function $B_{i,n}(u)$ is the classical Bernstein polynomial with n^{th} degree, which can be given by:

Int J Adv Manuf Technol (2015) 77:469–483
DOI 10.1007/s00170-014-6489-9

Received: 3 June 2014 /Accepted: 9 October 2014
Published online: 18 October 2014

$$B_{i,n}(u) = \frac{n!}{i!(n-i)!} u^i (1-u)^{n-i} \tag{2}$$

Using this definition, a cross-section profile can be described with the given control points $\{P_i\}$ and their weights $\{\omega_i\}$. Equation (1) provides a convenient approach to describe the geometrical profiles in the calculation process.

2.2 Geometric profiles generation algorithm

In the ISF process, the forming tool deforms the sheet in the vertical z direction level by level, incrementally obtains the final shape. Considering the prediction of part profile after the tool movement of each z-level, as the pre-described tool path is known, the cross sectional shape of part can be generated with forming parameters including tool radius R and the step down value dz.

For a typical two-pass ISF process, concerning the intermediate shapes in the first pass as shown in Fig.1, when the tool center locates at O_N the geometric profile is composed of three parts: the deformed inclined wall (described by curve a-b), the contact region (described by curve b-c-d) and the unformed bottom area (described by curve d-e-f). When the tool moves down to the point O_{N+1} for the $N+1^{th}$ z-level, the wall a-b-c is further deformed and the original contact area c-d-e moves to c-g-h. The unformed bottom area e-f keeps unchanged and becomes h-i. Concerning the material movement in this process, the material at the region a-b and h-i is kept unchanged. The sheet d-e joins the deformation while the sheet b-c is left in the deformation process. In this way, the geometric profiles can be described based on the given tool position and radius.

Int J Adv Manuf Technol (2015) 77:469–483
DOI 10.1007/s00170-014-6489-9

Received: 3 June 2014 /Accepted: 9 October 2014
Published online: 18 October 2014

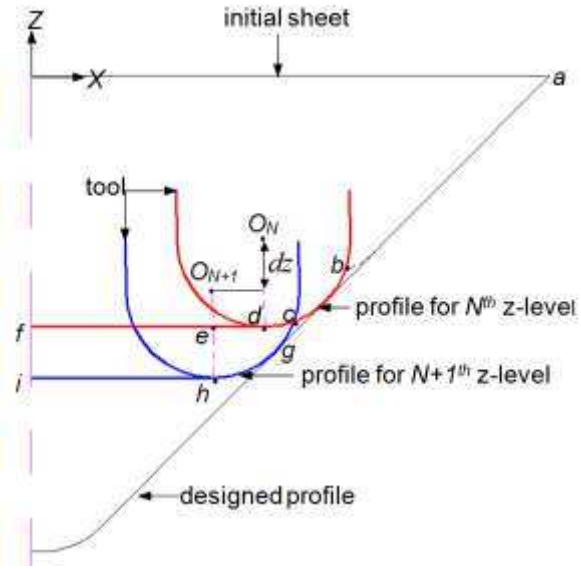

Fig.1 Generation algorithm of geometric profiles in the first pass

Concerning the second pass, the geometry of the tool motion path in the cross-section can also be obtained by offsetting the designed profile of the second pass. As shown in Fig. 2, if the geometric profile for the N^{th} z-level has already been computed and O_N is the tool center, the tool center O_{N+1} for the $N+1^{th}$ z-level can be calculated according to the designed tool path with the step down value dz. Depending on the relative position of the geometric profile for the N^{th} z-level and the tool contour for the $N+1^{th}$ z-level, the relationship between the geometric profiles and tool can be divided into two cases as shown in Fig.2.

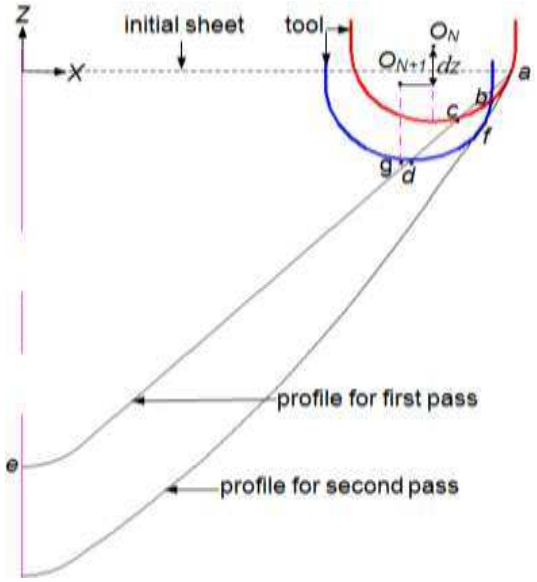

(a) The lowest point of the tool for the $N+1^{th}$ z-level is over the geometric profile for the N^{th} z-level

Int J Adv Manuf Technol (2015) 77:469–483
DOI 10.1007/s00170-014-6489-9

Received: 3 June 2014 /Accepted: 9 October 2014
Published online: 18 October 2014

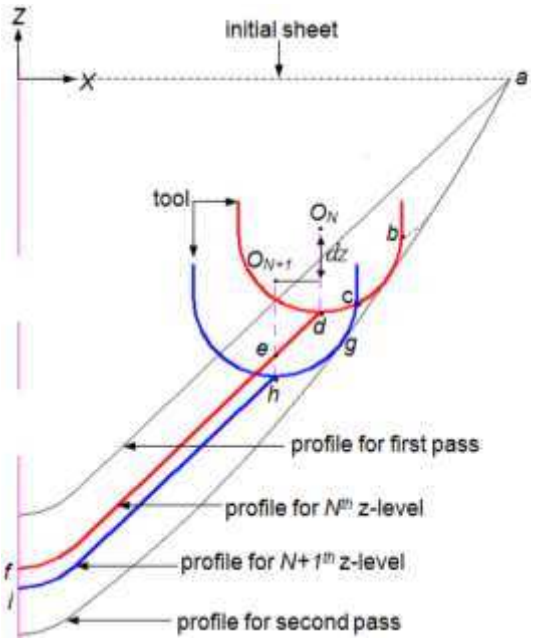

(b) The lowest point of the tool for the N+ 1^{th} z-level is below the geometric profile for the N^{th} z-level

Fig.2 Geometric profiles generation in the second pass (a) the lowest point of the tool for the N+ 1^{th} z-level is over the geometric profile for the N^{th} z-level ; (b) the lowest point of the tool for the N+ 1^{th} z-level is below the geometric profile for the N^{th} z-level

As shown in Fig.2 (a), the tool tip g for N+ 1^{th} z-level is above the geometrical profile of previous N^{th} z-level a-b-c-d-e. In this case, the sheet profile for N+ 1^{th} z-level can be described by the curve a-b-f-d-e, in which the curve a-b is the deformed area, b-c-d deforms to b-f-d and d-e is still the un-deformed sheet area.

As shown in Fig.2 (b), the tool tip h for N+ 1^{th} z-level is below the geometrical profile of previous N^{th} z-level a-b-c-d-e-f. In this case, the sheet profile for N+ 1^{th} z-level can be described by the curve a-b-c-g-h-i, in which the curve a-b-c is the deformed area, c-d-e moves to c-g-h, and e-f moves to h-i as rigid body motion.

In the multi-pass ISF process, if the intermediate shapes are not properly designed, the tool and sheet may lose the contact due to the rigid body motion of un-deformed sheet below the tool, which results in an inaccurate final part geometry. In order to consider this effect in the proposed model, the minimum distance between the tool center and the geometric profiles will be calculated to determine the status of contact between the tool and sheet. As shown in Fig. 3, if this distance is greater than the tool radius, then contact is lost and the calculation process

Int J Adv Manuf Technol (2015) 77:469–483
DOI 10.1007/s00170-014-6489-9

Received: 3 June 2014 /Accepted: 9 October 2014
Published online: 18 October 2014

will stop.

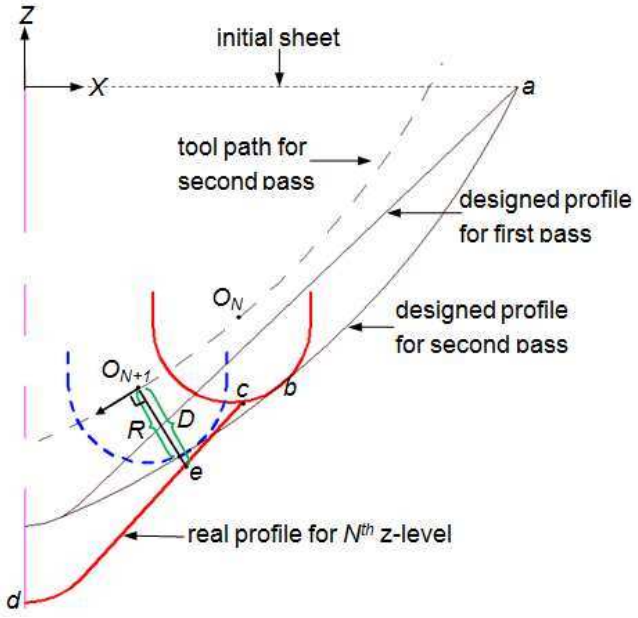

Fig. 3 The determination of contact between the tool and sheet

2.3 Backward tracing of material points

Based on the calculated shapes, the material motion may be traced according to the intermediate shape of each z-level. In this work, a backward tracing method is developed. In this method, the nodal point on the final predicted shape is traced back to dreamtime its position on the intermediate shapes and initial blank. It is assumed that the material point will move along its normal position on the surface in every transient time [19]. In this way, for any given point P on the final surface $N+1^{th}$ level, the point position on the previous surface of N^{th} level can be obtained by calculating the intersection point of the P's normal and the profile curve of N^{th} level. By repeating this process, the point P^{N-1} for $N\text{-}1^{th}$ z-level until the initial position P^0 can be calculated. This process can be illustrated as shown in Fig. 4.

Int J Adv Manuf Technol (2015) 77:469–483
DOI 10.1007/s00170-014-6489-9

Received: 3 June 2014 /Accepted: 9 October 2014
Published online: 18 October 2014

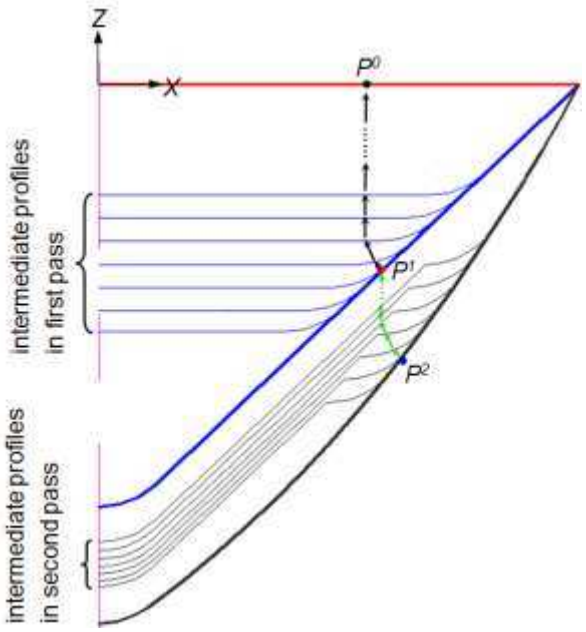

Fig. 4 The tracing of material points in the two-pass ISF process

According to the updated point positions after deformation, the thickness distribution can be calculated under the volume constancy assumption. In this work, for any two neighboring points P, Q on the blank, the thickness can be updated by:

$$t_{PQ}^{i+1} = t_{PQ}^{i} \cdot \frac{A_{PQ}^{i}}{A_{PQ}^{i+1}} \tag{3}$$

where t_{PQ}^{i} represents the sheet thickness while A_{PQ}^{i} represents the segment area between P and Q for pass number i. The segment area can be obtained from the coordinates of the calculated point position.

Int J Adv Manuf Technol (2015) 77:469–483
DOI 10.1007/s00170-014-6489-9

Received: 3 June 2014 /Accepted: 9 October 2014
Published online: 18 October 2014

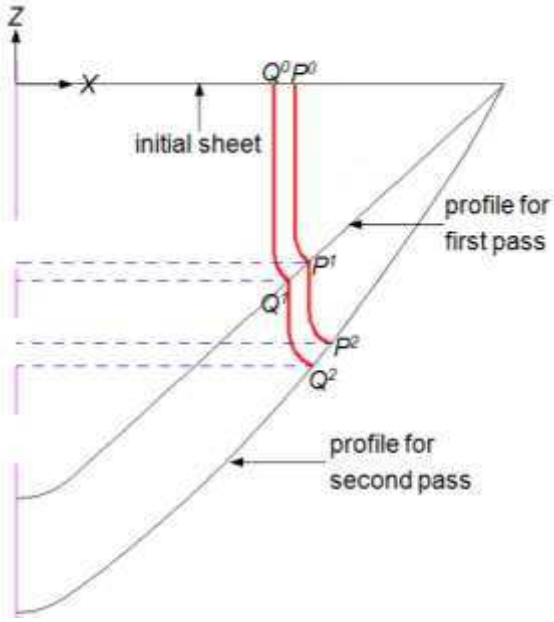

Fig. 5.The traces of two adjacent points of P and Q in two-pass ISF process

2.4 Development of thickness prediction program

In this work, an in-house software program is developed to predict the ISF thickness distribution. For any given initial shape and final profile, the thickness is calculated according to the developed method and the calculation procedure is illustrated in Fig. 6. As shown in the figure, the control points of the designed profile for the second pass is firstly imported and then a rational Bezier curve is generated to depict the designed profile. By offsetting a distance of tool radius R, the tool path can be obtained and the tool position at each z-level can be calculated with the step down value dz. With the new tool position, the contact state between the tool and sheet will be checked. If there is no contact between the tool and sheet, the forming process stops and the final geometric profile can be generated according to the current state. Otherwise, the geometric profile for the $N+1^{th}$ z-level is calculated according to Fig.2 (a) or Fig.2 (b) depending on the relative position of the geometric profile and the tool. In this way, the geometric profiles for each z-level deformation can be calculated. After the final geometric profile of the forming pass is generated, the tracing of material points on the surface of the part can be computed based on the algorithm illustrated in Fig.4. Then the final thickness distribution can be calculated by using the equation (3). In this way, the thickness distribution may be obtained.

Int J Adv Manuf Technol (2015) 77:469–483
DOI 10.1007/s00170-014-6489-9

Received: 3 June 2014 /Accepted: 9 October 2014
Published online: 18 October 2014

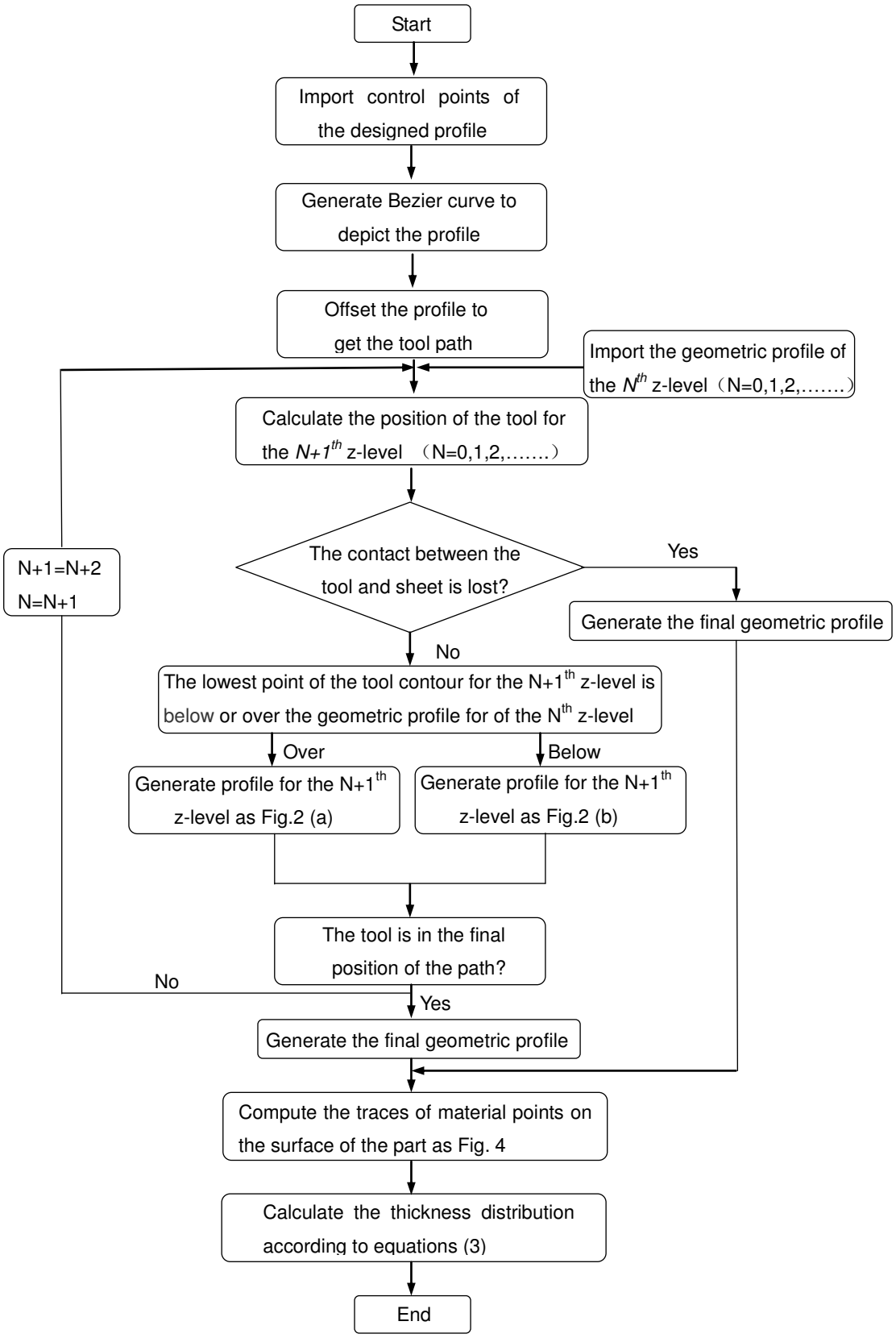

Fig. 6 Procedure to calculate the thickness distribution of multi-pass ISF process

Int J Adv Manuf Technol (2015) 77:469–483
DOI 10.1007/s00170-014-6489-9

Received: 3 June 2014 /Accepted: 9 October 2014
Published online: 18 October 2014

3. Experimental Validation

Using the developed geometric profiles generation, material deformation and thickness distribution calculation method, the final shape of part fabricated by multi-pass ISF technology can be predicted. To verify the developed thickness prediction approach, four different shapes including a cone shape with a constant forming angle, a parabolic cone, a non-axisymmetric part and a hemisphere were formed. The intermediate and final shapes and the final thickness distributions from analytical model and experiments were calculated and measured, respectively.

3.1 Experimental setup

The experiments were performed on a 3-axial CNC machine as shown in Fig. 7. A ball head tool with a radius of 5mm was used to form the parts with the feed rate of 2000 mm/min. Contour based tool path with a step down value of 0.2mm was generated and used for the four parts. Aluminum alloy AA5052 and AA1100 with initial thickness of 1mm had been used in the experiments. For the case1-3, AA5052 was employed in the experiments. For the fourth case with large forming angle, AA1100 was used to validate the effectiveness of the developed method. The initial size of the blank is 180×180mm. During the forming process, grease was employed as lubrication to reduce the friction between tool and sheet. Note that a backing plate had been placed at the bottom of blank to avoid the bending around the top edge of part in the forming process. In the experiments, depending on the forming steps, the part in each case are formed 2-4 times to ensure the experimental repeatability on both thickness and cross-sectional profiles. After forming, the cross-section of geometric profiles of finished parts are measured by using a KEYENCE® LK-G150 laser displacement sensor with a resolution of 0.01 μm as shown in Figure 8. It is worthwhile to mention that the on the top surface profiles are measured in the experiment while in the prediction, the tracing of material points are also implemented on the top surface of the part. In this way, the profiles measured and calculated at the same surface can be compared.

Int J Adv Manuf Technol (2015) 77:469–483
DOI 10.1007/s00170-014-6489-9

Received: 3 June 2014 /Accepted: 9 October 2014
Published online: 18 October 2014

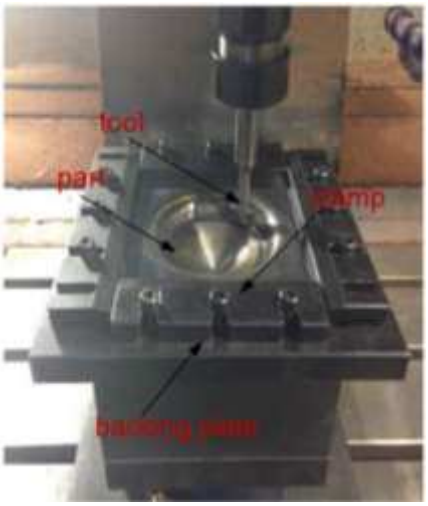

Fig.7 Experimental setup

Fig.8 Measurement of the part profile

3.2 Case1: a cone shape with a constant forming angle

In this case, a cone shape with a major diameter of 120mm and constant angle of 60° was employed to validate the developed method. Two forming passes had been designed to form the designed cone. In the first pass, a cone with a constant wall angle of 30° would be formed. In the second pass, the final shape would be formed as shown in Fig. 9. Fig. 10 shows the finished parts after each forming pass.

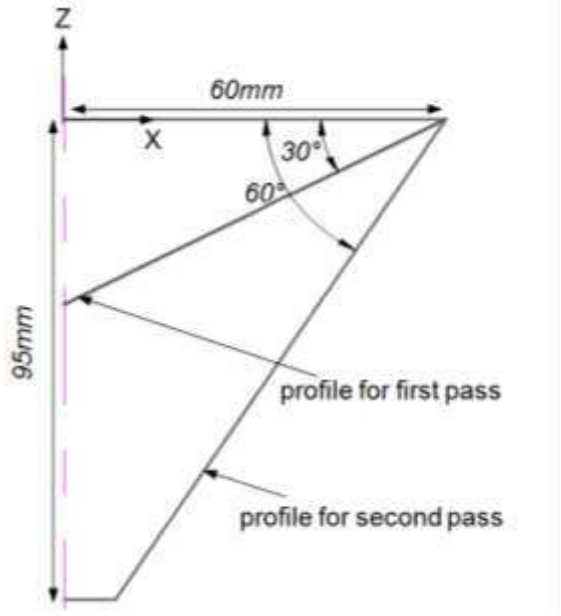

Fig.9 Geometric model of a cone shape with a constant forming angle

Int J Adv Manuf Technol (2015) 77:469–483
DOI 10.1007/s00170-014-6489-9

Received: 3 June 2014 /Accepted: 9 October 2014
Published online: 18 October 2014

(a) Part for the first pass (b) Part for the second pass

Fig.10 Formed parts: (a) part for the first pass; (b) part for the second pass

In order to compare the intermediate profile shapes, in the experiment, the ISF process was paused and the intermediate cross-section shapes were measured when the forming depth increased every 10mm. In this way, about 9 intermediate profiles are obtained and these profiles are compared with those obtained from the analytical prediction. In addition, the designed profile is also included in the comparison as reference. The comparison result is given in Fig.11. As can be seen from the figure, the predicted profile is quite close to the designed profile but some discrepancy can be observed for those measured in the experiment: the predicted profiles are about 1mm deeper than the experimental one. This discrepancy may be from two sources: 1) the initial bending at the top edge of the cone, which is not considered in the analysis. 2) Another factor may be from the cyclized loading: after the tool leaving a certain location, the spring back of sheet occurs. However, this spring back is not considered in the analysis as well.

Int J Adv Manuf Technol (2015) 77:469–483
DOI 10.1007/s00170-014-6489-9

Received: 3 June 2014 /Accepted: 9 October 2014
Published online: 18 October 2014

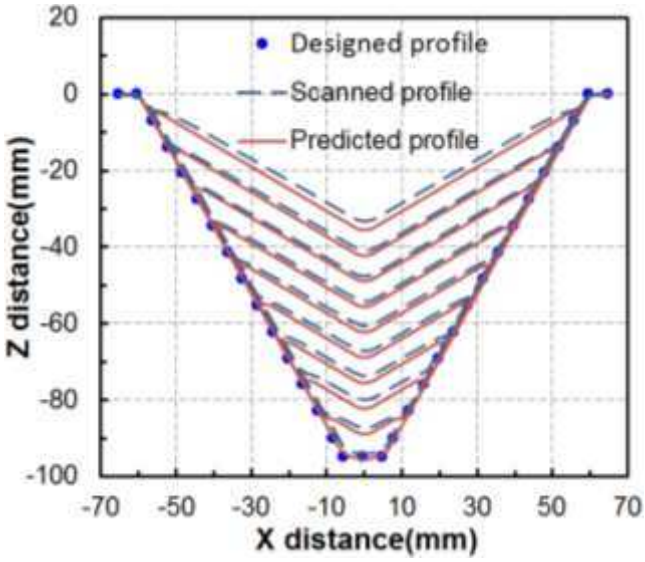

Fig.11 Comparison of the scanned geometric profiles with predicted geometric profiles

In order to measure the thickness distribution, the thicknesses of the formed parts were marked at an interval of 2mm on the initial sheet surface and then the thicknesses were measured according to these marks on the formed parts. Fig. 12 compares the thickness distributions of the physical formed parts and the predicted results by both the developed method and the Sine law for the first and second passes. As can be seen in the figure, the prediction accuracy of Sine law is obvious worse than the developed method. Concerning the first pass, as shown in Fig.12 (a), accurate prediction can be obtained by comparing the experimental result, except for the edge of cone, where the predicted thickness changes rapidly while the actual thickness decreases gradually. This may be attributed to that the developed method does not consider the bending effect. Concerning the second pass, the predicted result is still effective, although some deviations can be observed at the top edge of the cone. The bending effect shows larger influence on the thickness at the edge of the cone, where the thickness changes rapidly and a thinning band can be observed in the actual formed parts (see Fig.10b). Generally, the developed method suggests good thickness prediction accuracy for multi-pass forming of a cone shape with constant wall angle.

Int J Adv Manuf Technol (2015) 77:469–483
DOI 10.1007/s00170-014-6489-9

Received: 3 June 2014 /Accepted: 9 October 2014
Published online: 18 October 2014

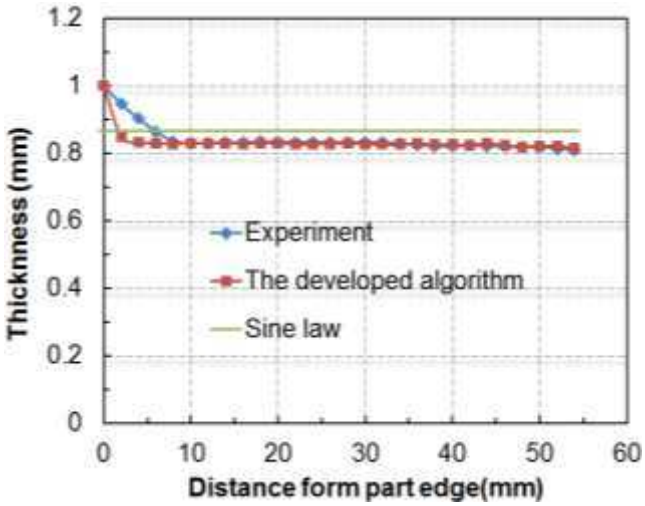

(a)Thicknesses for the first pass

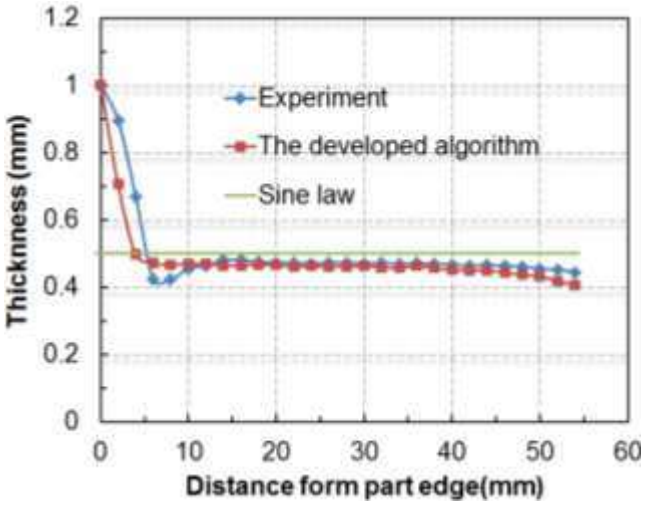

(b) Thicknesses for the second pass

Fig.12 Comparison between the experimental thickness distributions and the predicted results: (a) thicknesses for the first pass; (b) thicknesses for the second pass

3.3 Case2: a parabolic cone

In the second case problem, a parabolic cone with varied wall angle was employed in the analysis. Similar to the previous case, the major diameter of the cone is 120mm. Two forming steps were employed in the analysis. In the first step, a cone with constant angle of 45° was formed. In the second step, ISF was implemented to finalize the part to the designed geometry as shown in Fig.13. Fig.14 shows the finished parts in the two forming steps.

Int J Adv Manuf Technol (2015) 77:469–483
DOI 10.1007/s00170-014-6489-9

Received: 3 June 2014 /Accepted: 9 October 2014
Published online: 18 October 2014

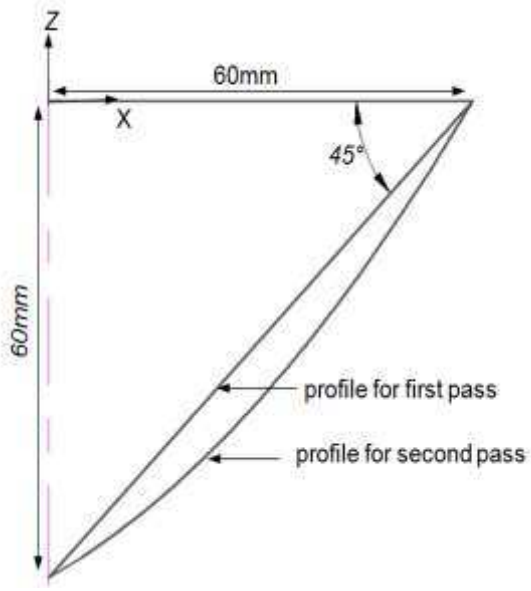

Fig.13 Geometric model of a parabolic cone

(a) Part for the first pass (b) Part for the second pass

Fig.14 Formed parts: (a) part for the first pass; (b) part for the second pass

It is worthwhile to note that, the first step and second step are designed with the same depth as shown in the Fig.13. This kind of pass design will result in the rigid body motion of sheet at the second step. This rigid body motion will result in the losing of contact between tool and sheet. This could also be observed in Cao's work [13]. Concerning the rigid body motion in this case, as shown in Fig.15b, the stepped feature can be observed due to the loss of contact between the tool and sheet.

Concerning the intermediate profile shape prediction, in the experiments, the intermediate profile shapes with the tool at different depths were measured during the second

Int J Adv Manuf Technol (2015) 77:469–483
DOI 10.1007/s00170-014-6489-9

Received: 3 June 2014 /Accepted: 9 October 2014
Published online: 18 October 2014

forming step. Fig.15 compares the scanned, predicted and designed geometric profiles. As can be seen from the figure, only little difference can be observed between the scanned profile and predicted profile, which suggests relatively high prediction accuracy.

Concerning the designed profile and the predicted profile as shown in Fig. 15(d), obvious difference can be observed: no stepped feature was expected in the design. However, this feature was captured by the developed program and it also occurred in the actual case. The discrepancy between the final forming depth of the prediction and the experiment is very little. This result suggested the satisfactory prediction of rigid body motion of the developed method.

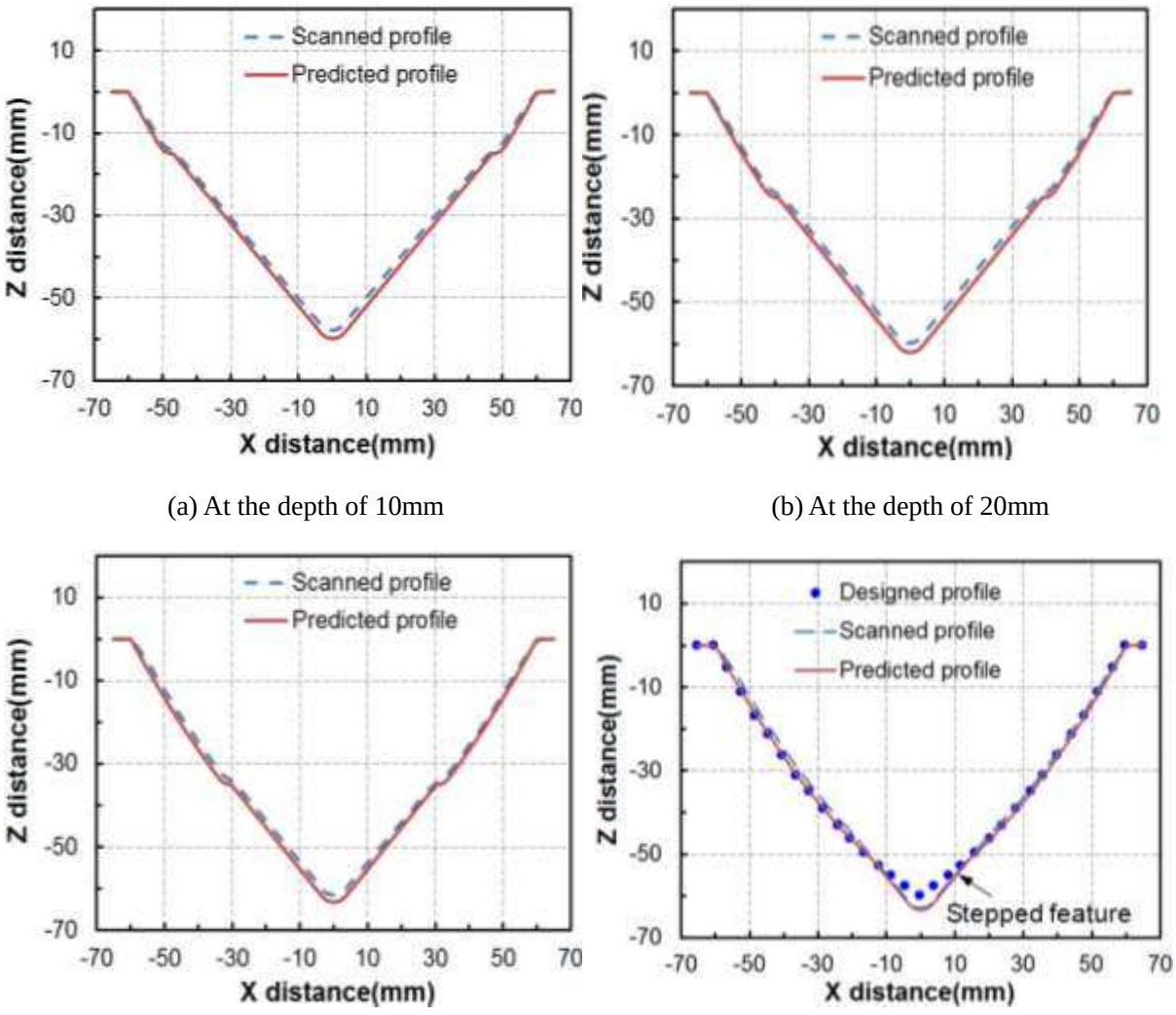

(a) At the depth of 10mm

(b) At the depth of 20mm

(c) At the depth of 30mm

(d) Final position

Fig.15 Comparison of the scanned geometric profiles with predicted geometric profiles: (a) at the depth of 10mm; (b) at the depth of 20mm; (c) at the depth of 30mm; (d) the final position

Int J Adv Manuf Technol (2015) 77:469–483
DOI 10.1007/s00170-014-6489-9

Received: 3 June 2014 /Accepted: 9 October 2014
Published online: 18 October 2014

Concerning the thickness distribution, as can be seen from Fig. 16(a), the Sine law does not show good accuracy while the developed method is more accurate. Concerning the first forming step, the developed program suggests accurate result. In the second step, the prediction and the actual results have the same trend in thickness distribution. At the edge of cone, the prediction is not very accurate as the sheet thinning may be affected by bending effect. On the part wall, the prediction result is close to experimental result. The maximum discrepancy is about 0.085mm, which represents the prediction error of about 8%. This case study suggests that in the condition of variable wall angle, the developed method is still effective in thickness prediction.

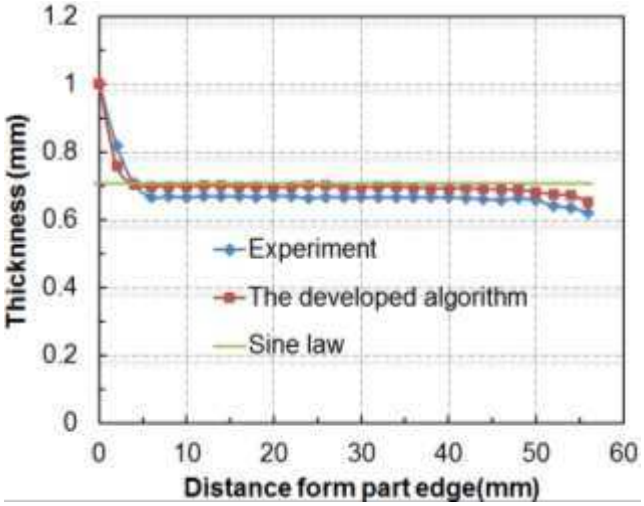

(a)Thicknesses for the first pass

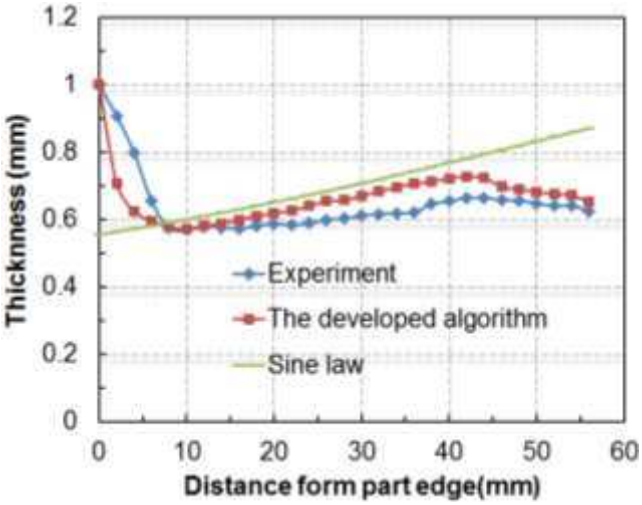

(b) Thicknesses for the second pass

Fig.16 Comparison between the experimental thickness distributions and the predicted results: (a) thicknesses for the first pass; (b) thicknesses for the second pass

Int J Adv Manuf Technol (2015) 77:469–483
DOI 10.1007/s00170-014-6489-9

Received: 3 June 2014 /Accepted: 9 October 2014
Published online: 18 October 2014

3.4 Case3: a non-axisymmetric part

In the above two cases, axisymmetric parts were employed in the analysis. In order to examine the robustness of the developed method and program， a part with different cross-section shapes was designed as shown in Fig.17. In the ISF process, two forming stages were employed as given in the figure. Fig. 18 shows the final formed parts.

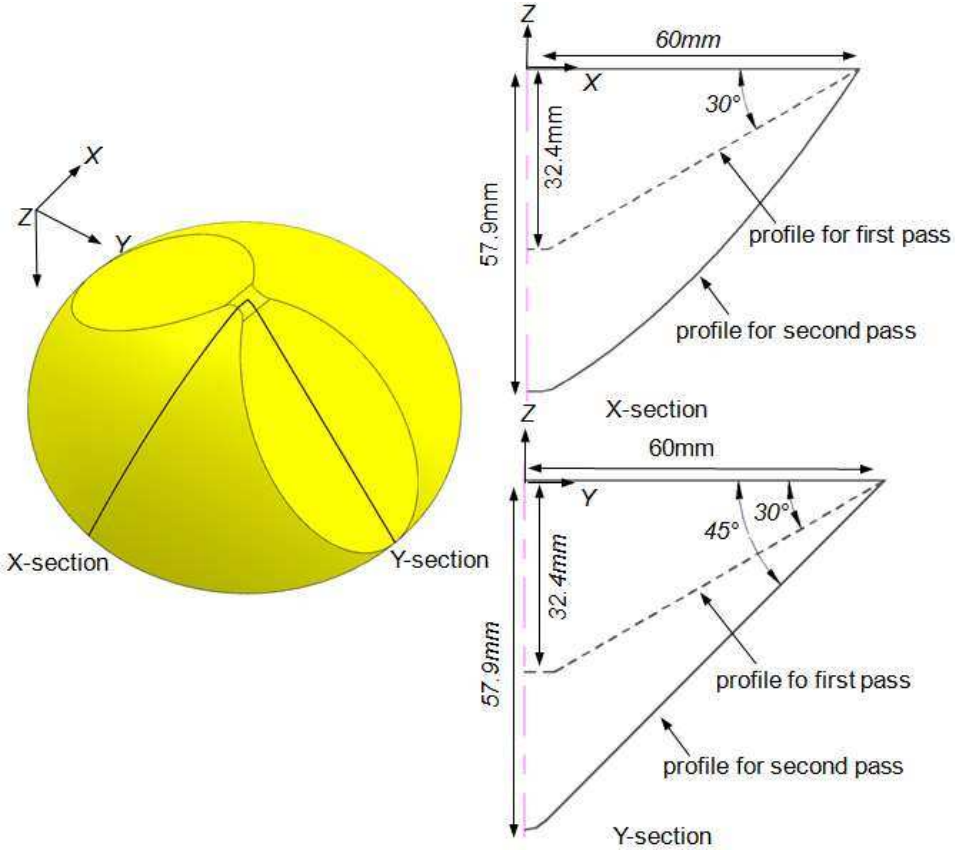

Fig.17 Geometric model of a non-axisymmetric part

(a) Part for the first pass (b) Part for the second pass

Fig.18 Formed parts: (a) part for the first pass; (b) part for the second pass

Int J Adv Manuf Technol (2015) 77:469–483
DOI 10.1007/s00170-014-6489-9

Received: 3 June 2014 /Accepted: 9 October 2014
Published online: 18 October 2014

Fig. 19 compares the final geometry of the formed part. As can be seen from the figure, the prediction of final geometry by using the developed program is quite effective. The difference at the top edge is because of obvious bending observed for the actual formed part. In the comparison, the maximum difference occurs at the bottom of the part, with maximum distance of about 1.8mm.

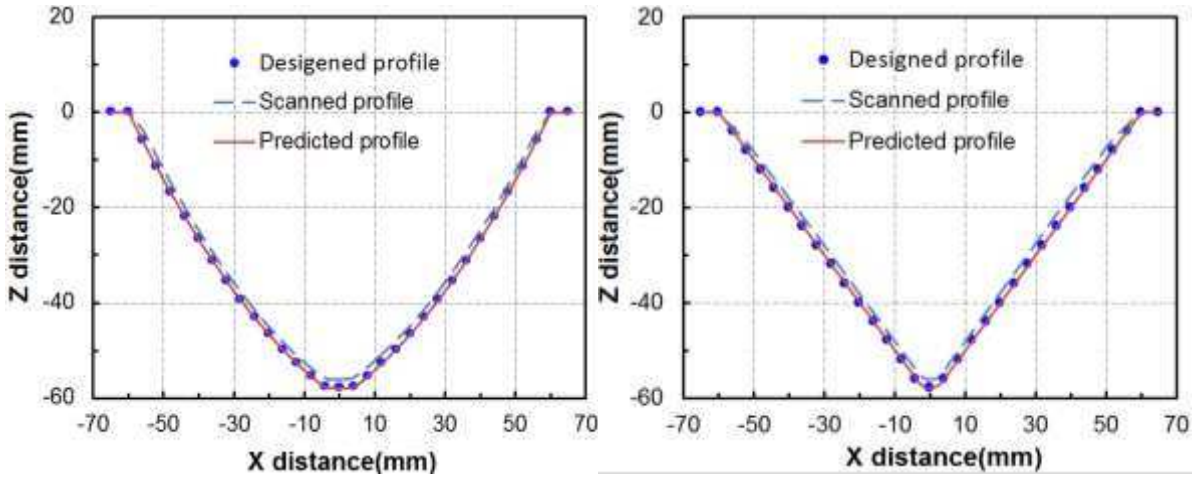

(a) Final profile for the X-section (b) Final profile for the Y-section

Fig.19 Comparison of the scanned geometric profiles with predicted geometric profiles: (a) final profile for the X-section; (b) final profile for the Y-section

Concerning the thickness distribution prediction, both the developed method and the Sine law are accurate for the first forming step. At the second stage, the prediction and the actual results have the similar trend in thickness distribution (see Fig.20 (b) and (c)). At the edge of cone, the predicted values are thinner than the actual result for the bending effect is not considered in the analysis. Beside this, the thicknesses calculates from the developed method are thicker than the measured thicknesses of part. Taking Fig.20 (c) as examples, the maximum discrepancy of Y –section occurs at the distance of 30mm from part edge, with the maximum value of about 0.084mm, which suggests the prediction error of about 8%. Although the Sine law shows the similar trend in prediction, the results is even worse at the edge of the cone.

Int J Adv Manuf Technol (2015) 77:469–483
DOI 10.1007/s00170-014-6489-9

Received: 3 June 2014 /Accepted: 9 October 2014
Published online: 18 October 2014

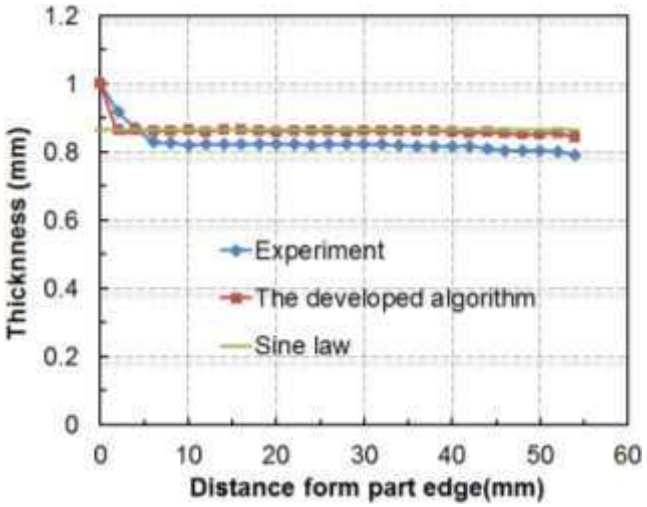

(a)Thicknesses for the first pass

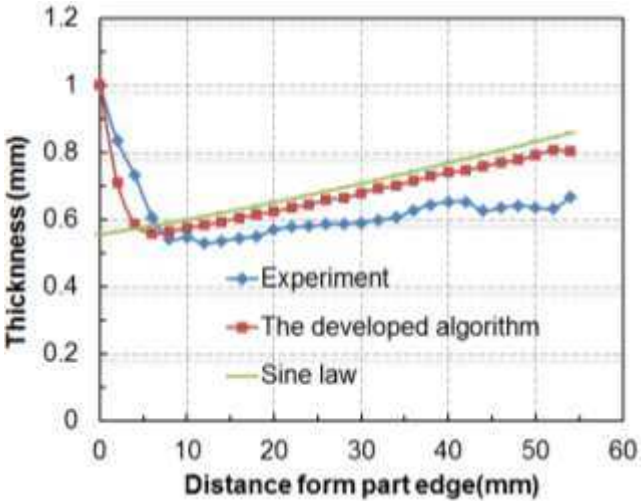

(b)Thicknesses for the second pass of X-section

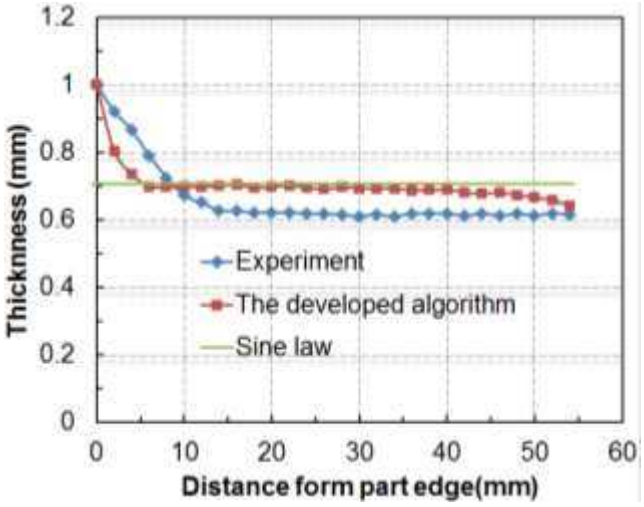

(c) Thicknesses for the second pass of Y-section

Fig.20 Comparison between the experimental thickness distributions and the predicted results: (a) thicknesses for the first pass; (b) thicknesses for the second pass of X-section; (c) thicknesses for the second pass of Y-section

Int J Adv Manuf Technol (2015) 77:469–483
DOI 10.1007/s00170-014-6489-9

Received: 3 June 2014 /Accepted: 9 October 2014
Published online: 18 October 2014

3.5 Case 4: a hemisphere

In cases 1-3, only two forming stages were employed in the analysis. To further validate the robustness of the development method under the case with four forming steps and wall angle of 90º, a hemisphere part with diameter of 118mm had been employed. Four forming stages had been designed as shown in Fig. 21. In order to achieve the maximum wall angle of 90º, AA1100 material was employed. Fig. 22 shows the finished parts after each forming stages.

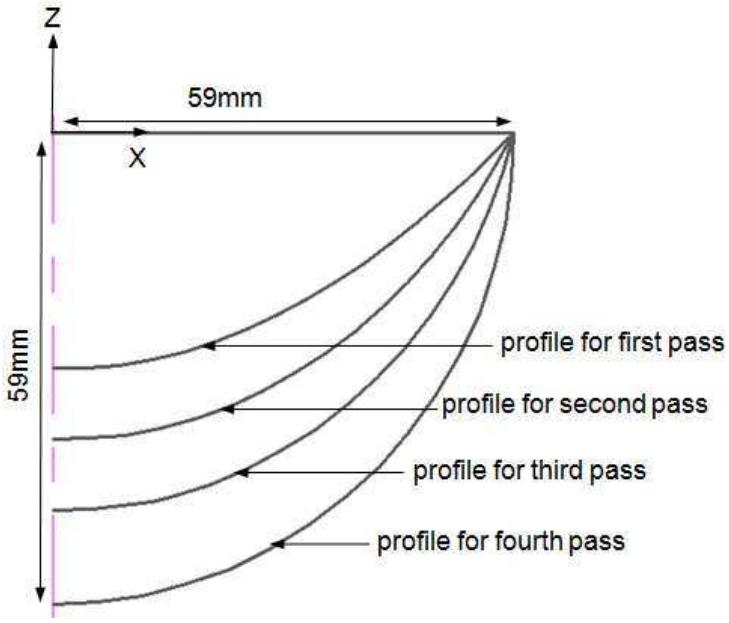

Fig.21 Geometric model of a hemisphere

(a) First forming pass

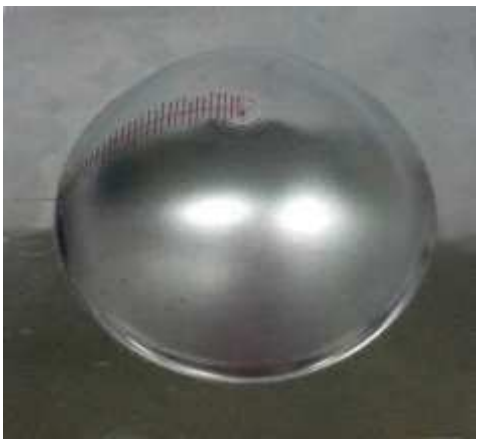

(b) Second forming pass

Int J Adv Manuf Technol (2015) 77:469–483
DOI 10.1007/s00170-014-6489-9

Received: 3 June 2014 /Accepted: 9 October 2014
Published online: 18 October 2014

(c) Third forming pass (d) Final forming pass

Fig.22 Formed parts: (a) First forming step; (b) Second forming step

(c) Third forming step; (d) Final forming step

Fig. 23 compares the scanned, predicted and designed geometric profiles the end of the second, the third and the fourth forming stages. In addition, intermediate scanned and predicted profiled near the beginning of each forming stage were also compared for further validation. As can be seen from the figure, the predicted profiles are quite close to those measured in the experiments, which suggests the robustness of the developed program on geometrical shape prediction.

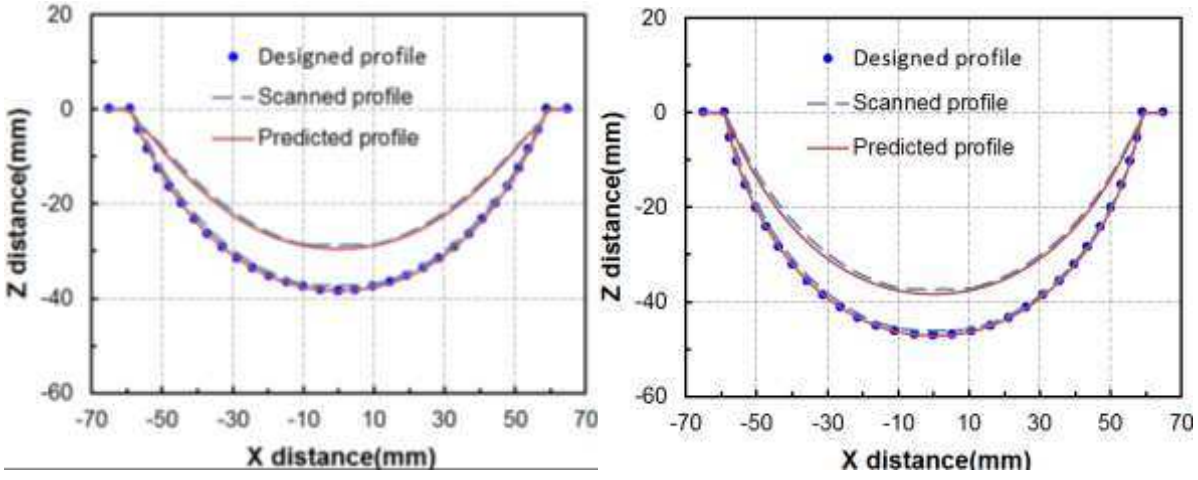

(a) Profiles for the second forming pass (b) Profiles for the third forming pass

Int J Adv Manuf Technol (2015) 77:469–483
DOI 10.1007/s00170-014-6489-9

Received: 3 June 2014 /Accepted: 9 October 2014
Published online: 18 October 2014

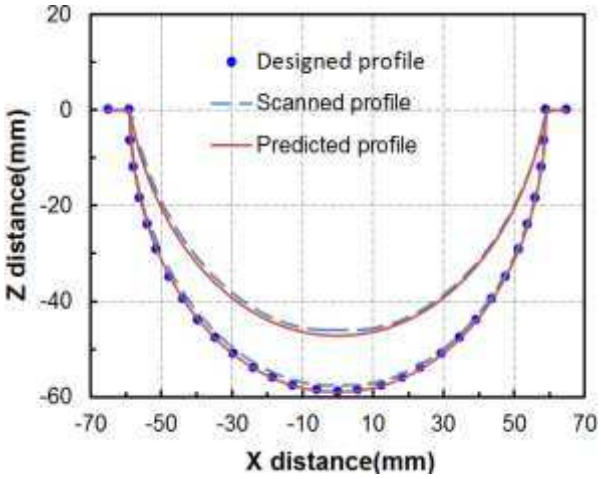

(c) Profiles for the fourth forming pass

Fig.23 Comparison of the scanned geometric profiles with predicted geometric profiles: (a) profiles for the second forming pass; (b) profiles for the third forming pass; (c) profiles for the fourth forming pass

Concerning the thickness distribution, Fig. 24 compares those from the physical formed parts and the predictions by both the developed method and the Sine law for all the forming stages. As can be seen in the figure, very accurate prediction can be obtained at the initial forming stages. However, with the increasing of forming steps, the prediction accuracy reduces due to the error accumulation. Concerning the Sine law, the prediction result obtains from the Sine law is much worse than the developed method. For the third step as shown in Fig. 24(c), obvious difference between the experiment and Sine law can be observed, while the maximum discrepancy is over 0.15mm while that for the developed method is less than 0.1mm. For the fourth step, the error of the Sine law become over 0.2mm while that for the developed method is about 0.1mm, except for the points that near the edge of part: the minimum thickness predicted by the developed method is about 0.2mm while in the actual case, the minimum point is about 0.35mm. This discrepancy may be attributed to the double effect from bending and error accumulation. From this case, it may be obtained that the accuracy may reduce with the increase of forming step, as the thickness calculation is based on the previous results. Generally speaking, for a three-step forming, the accuracy is satisfactory but for four-step forming, the prediction error may be over 0.1mm.

Int J Adv Manuf Technol (2015) 77:469–483
DOI 10.1007/s00170-014-6489-9

Received: 3 June 2014 /Accepted: 9 October 2014
Published online: 18 October 2014

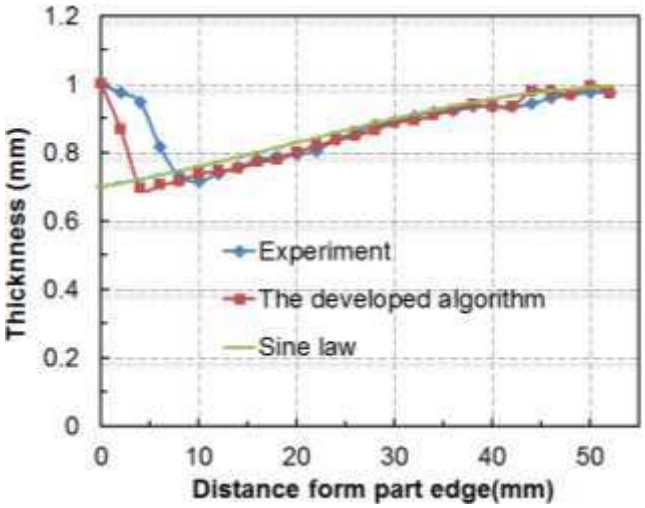

(a)Thicknesses for the first pass

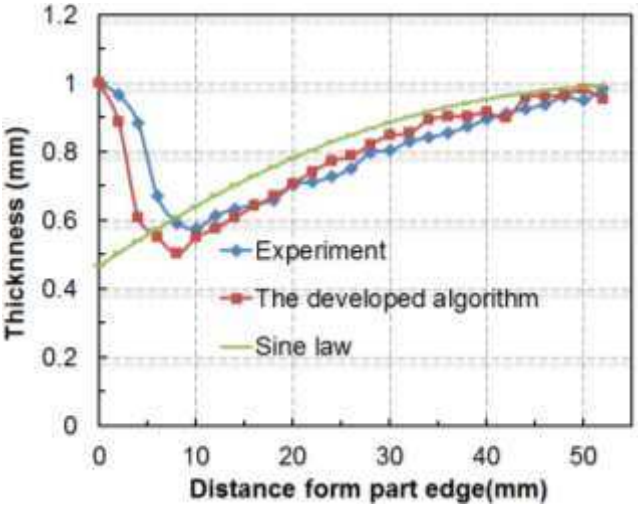

(b)Thicknesses for the second pass

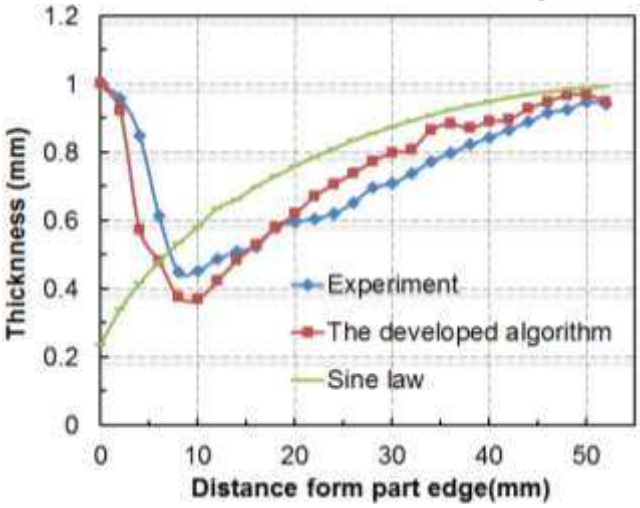

(c)Thicknesses for the third pass

Int J Adv Manuf Technol (2015) 77:469–483
DOI 10.1007/s00170-014-6489-9

Received: 3 June 2014 /Accepted: 9 October 2014
Published online: 18 October 2014

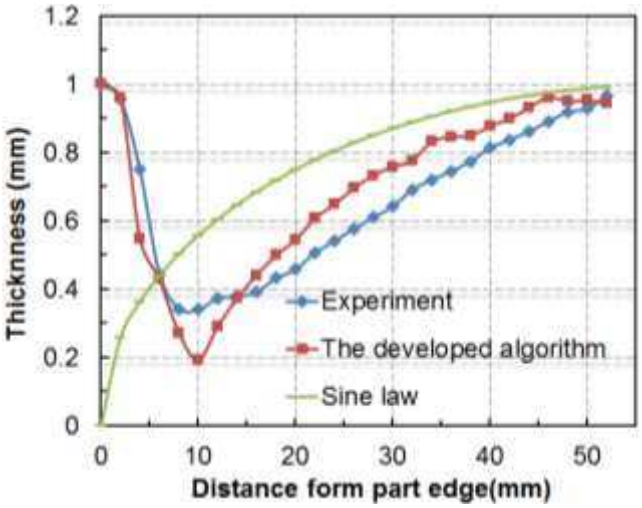

(d)Thicknesses for the fourth pass

Fig.24 Comparison between the experimental thickness distributions and the predicted results: (a) thicknesses for the first pass; (b) thicknesses for the second pass; (c) Thicknesses for the third pass; (d)Thicknesses for the fourth pass

3.6 Discussion of results

The developed thickness prediction method is a geometric approach based on the calculation of intermediate geometric profiles of each z-level and the trace of material point in the forming process. The examples of a basic cone shape, a parabolic cone shape, a non-axisymmetric shape and a hemisphere suggested the satisfactory prediction accuracy, which demonstrated the robustness of the developed method. Comparing to the conventional Sine law calculation, the developed method showed more accurate prediction results. Comparing to the FE approach, the developed method is much more efficient. In this way, a good balance between the calculation accuracy and efficiency can be achieved in the prediction of multi-pass ISF thickness distribution.

In this study, it is found that the thickness prediction accuracy also depends on the prediction of the intermediate geometric profiles, the trace of material point and the accumulation of errors, which may also be affected by the bending effect during the process as well as the sheet material property. The discrepancy between the prediction and experiments may be due to these factors.

Concerning the future work, further investigation is necessary in the following aspects:

Int J Adv Manuf Technol (2015) 77:469–483
DOI 10.1007/s00170-014-6489-9

Received: 3 June 2014 /Accepted: 9 October 2014
Published online: 18 October 2014

(1) To consider the sheet bending effect so that the thickness distribution close to the edge of the part can be predicted.

(2) To introduce the plasticity theory into the sheet deformation calculation, so that it can provide a more accurate prediction in the cases that the sheet thickness is strongly affected by the material behavior, e.g. prediction of the thinning band.

4. Conclusions

In this paper, an efficient thickness prediction method for multi-pass incremental forming is proposed. By using the developed method, the geometric profiles, the positions and thickness distribution of four formed parts using multi-step ISF process are calculated. To validate the proposed method, four different geometrical shapes including a basic cone shape, a parabolic cone shape, a non-axisymmetric shape and a hemisphere are produced. The geometric profiles and the thickness distributions of the formed shapes are measured to be compared with those obtained from the developed method. The agreement between the analytical calculation and experimental validation demonstrates the advantages of the developed method as outlined as following:

(1) The thickness prediction method for multi-pass incremental forming processes produces relatively accurate results for both the final geometrical shape and the corresponding thickness distribution, for examples of the axisymmetric and non-axisymmetric parts.

(2) The stepped features due to rigid body motion during the ISF process can also be predicted accurately by the developed method.

(3) This method is very computational efficient. It could produce the thickness distribution prediction in minutes, much faster than the conventional FE approach.

Acknowledgement

The authors are grateful for the financial support provided by National Key Specific Science & Technology Program from Ministry of Industry and Information Technology of China through Grant 2011ZX04016-051, the EU FP7 Marie Curie International Incoming Fellowship Program (628055 & 913055) and the EU Marie Curie Actions – MatProFuture Project (FP7-PEOPLE-2012-IRSES-318968).

Int J Adv Manuf Technol (2015) 77:469–483
DOI 10.1007/s00170-014-6489-9

Received: 3 June 2014 /Accepted: 9 October 2014
Published online: 18 October 2014

References

1. Jeswiet J, Micari F, Hirt G, Bramley A, Duflou J, Allwood J（2005）Asymmetric Single Point Incremental Forming of Sheet Metal. CIRP Ann Manuf Technol 54（2）：88-114
2. Malhotra R, Xue L, Belytschko T, Cao J（2012）Mechanics of fracture in single point incremental forming. J Mater Process Technol 212（7）:1573-1590
3. Ambrogio G, De Napoli L, Filice L, Gagliardi F, Muzzupappa M（2005）Application of Incremental Forming process for high customised medical product manufacturing. J Mater Process Technol 162-163：156-162
4. Micari F, Fratini L, Governale A, Lo Franco A, Panzeca A（2007）Incremental forming process for the accomplishment of automotive details. Key Eng Mat, 344：559-566
5. Iseki H, Kato K,Sakamoto S（1989） Flexible Forming Method Using Ball Roller. Proc. 40th Japanese Joint Conf. for Technology of Plasticity (in Japanese) 41-44
6. Matsubara S（1994）Incremental backward bulge forming of a sheet metal with a hemispherical head tool. Journal of JSTP 35: 1311–1316
7. Smith J, Malhotra R, Liu W. K, Cao J (2013) Deformation mechanics in single-point and accumulative double-sided incremental forming. Int J Adv Manuf Technol 69:1185-1201
8. Duflou J.R, Callebaut B, Verbert J, De Baerdemaeker H(2007) Laser Assisted Incremental Forming: Formability and Accuracy Improvement. CIRP Ann Manuf Technol 56(1): 273-276
9. Fan G.Q, Sun F.T, Meng X.G, Gao L, Tong G.Q(2010) Electric hot incremental forming of Ti-6Al-4V titanium sheet. Int J Adv Manuf Technol 49:941-947
10. Iseki H(2001) Flexible and incremental bulging of sheet metal using high-speed water jet. JSME Int J 44(2):486-493
11. Li J.C, Hu J.B,Pan J.J, Geng P (2012) Thickness distribution and design of a multi-stage process for sheet metal incremental forming. Int J Adv Manuf Technol 62(9-12):981-988
12. Skjoedt M, Bay N, Endelt B, Ingarao G(2008), Multi stage strategies for single point incremental forming of a cup. Int J Mater Form

Int J Adv Manuf Technol (2015) 77:469–483
DOI 10.1007/s00170-014-6489-9

Received: 3 June 2014 /Accepted: 9 October 2014
Published online: 18 October 2014

13. Malhotra R, Bhattacharya A, Kumar A, Reddy N.V, Cao J(2011) A new methodology for multi-pass single point incremental forming with mixed toolpaths. CIRP Ann Manuf Technol 60(1): 323-326
14. Zhang C, Xiao H.F, Yu D.H(2013) Incremental forming path-generated method based on the intermediate models of bulging simulation. Int J Adv Manuf Technol 67(9-12):2837-2844
15. Hussain G, Gao L(2007) A novel method to test the thinning limits of sheet metals in negative incremental forming. Int J of Mach Tool Manuf 47(3-4):419-435
16. Kitazawa K, Nakanes M, Hemi-ellipsoidal stretch expanding of aluminum sheet by CNC incremental forming process with two path method. J Japan Ins Light Met 47:440–445
17. Kitazawa K, S.H, Sumio Y (2001) Hemispherical stretch-expanding of aluminum sheet by computerized numerically controlled incremental forming process with two path method. J Japan Ins Light Met 46:219 -224
18. Van Houtte P, Van Bael A, He S, Duflou J.R, Szekeres A, Henrard C, Habraken A.M(2005) Finite element modeling of incremental forming of aluminum sheets. Adv Mat Res 6:525-532
19. Bambach M(2010) A geometrical model of the kinematics of incremental sheet forming for the prediction of membrane strains and sheet thickness. J Mater Process Technol 210(12):1562-1573
20. Duflou J.R, Verbert J, Belkassem B, Gu J, Sol H, Henrard C, Habraken A.M(2008) Process window enhancement for single point incremental forming through multi-step toolpaths. CIRP Ann Manuf Technol 57(1):253-256
21. Filice L(2006) A phenomenology-based approach for modeling material thinning and formability in incremental forming of cylindrical parts. Proc. IMechE 220:1449-1455
22. He S, Gu J, Sol H, Van Bael A, Van Houtte P, Tunckol Y, Duflou J.R(2007) Determination of Strain in Incremental Sheet Forming Process. Key Eng Mat 344:503-510
23. Ji Y.H,Park J.J(2008) Formability of magnesium AZ31 sheet in the incremental forming at warm temperature. J Mater Process Technol 201(1-3):354-358

Int J Adv Manuf Technol (2015) 77:469–483
DOI 10.1007/s00170-014-6489-9

Received: 3 June 2014 /Accepted: 9 October 2014
Published online: 18 October 2014

24. Fang Y, Lu B, Chen J, Xu D.K, Ou H(2014) Analytical and experimental investigations on deformation mechanism and fracture behavior in single point incremental forming. J Mater Process Technol 214:1503-1515

25. Piegl L, Tiller W (1996) The Nurbs Book